Communication

Not peer-reviewed version

Synthetic Data-Driven Exoskeleton Control via Contralateral Gait Fusion for Variable-Speed Walking

Jingshu Shi [†] , Hongwu Zhu [*,†] , Yifei Yang , Bowen Liu , Xingjun Wang [*]

Posted Date: 25 March 2026

doi: 10.20944/preprints202603.2037.v1

Keywords: data-driven; exoskeleton; reinforcement learning; sim-to-real transfer; contralateral gait

 doi:10.20944/preprints202603.2037.v1

Communication

Synthetic Data-Driven Exoskeleton Control via Contralateral Gait Fusion for Variable-Speed Walking

Jingshu Shi [1,†], Hongwu Zhu [2,*,†], Yifei Yang [1], Bowen Liu [2] and Xingjun Wang [1,*]

[1] Shenzhen International Graduate School, Tsinghua University Shenzhen 518055, China

[2] Innovation Department Skyworth Digital Co., Ltd Shenzhen 518000, China

* Correspondence: zhuhongwu0918@gmail.com (H.Z.); wang.xingjun@sz.tsinghua.edu.cn (X.W.)

† These authors contributed equally to this work.

Abstract

Data-driven exoskeletons promise adaptive augmentation of human mobility. Yet their widespread adoption is hindered by labor-intensive biomechanical data collection and extensive manual tuning. This study presents a highly efficient, simulation-generated synthetic data approach. It also designs a model-free algorithm for variable-speed walking to validate the method. We leveraged an Adversarial Motion Priors (AMP) agent to learn stylized walking within a massively parallel, physics-based simulation. The resulting high-fidelity data were collected and validated against OpenSim inverse dynamics pipelines. A novel CNN-Transformer architecture was developed to map contralateral swing-phase sensor data to variable-length push-off torque profiles. This enables real-time, adaptive torque assistance for exoskeletons. Experimental validation on a custom ankle exoskeleton demonstrated robust sim-to-real transferability. The system achieved approximately 85% torque prediction accuracy across speeds ranging from 0.6 to 1.75 $m \cdot s^{-1}$. The controller significantly reduced user ankle positive mechanical work, thereby lowering metabolic demand. Furthermore, our multi-sensor configuration exhibited inherent fault tolerance, ensuring safe operation even under partial sensor failure. By replacing handcrafted control strategies with a scalable, data-driven approach, this work offers a practical pathway toward deploying autonomous exoskeletons in unconstrained, real-world environments.

Keywords: data-driven; exoskeleton; reinforcement learning; sim-to-real transfer; contralateral gait

1. Introduction

Powered exoskeletons hold transformative potential for augmenting human mobility [1–4]. Yet their widespread adoption is stifled by the rigidity of conventional control architectures. Dominant hierarchical approaches rely on high-level discrete task classification to trigger mid-level phase-based spline torque profiles [5–8]. Such methods is inherently incapable of accommodating unstructured, non-cyclic, or transitory movements that characterize daily life. Moreover, optimizing human-in-the-loop control parameters for each specific task and participant typically demands laborious trials or metabolic cost measurements [9,10]. These handcrafted, task-specific controllers fail to generalize. This creates an urgent need for a versatile strategy that operates without explicit task classification or exhaustive manual tuning.

Autonomous classifiers have been adopted to enable mode transitions between high-level assistive strategies. Human-in-the-loop optimization utilized respirometry measure as the metabolic cost. And control law optimization could be online solved via repeated laboratory trails including walking and running [2]. When replaced the above cost with a data-driven classifier, the optimization process can be performed rapidly in real-world conditions [11]. For high-level control, Data-driven models can estimate more high-level states compared with physics-driven models classifier [12]. A data-driven

 doi:10.20944/preprints202603.2037.v1

model can continuously classify environment, and estimate the phase, phase rate, stride length during locomotion [13,14]. Computer vision and deep learning was leveraged to classify environments and estimate terrains in both indoor and outdoor settings outdoors [15,16]. Proprioceptive sensors provide kinematic data for neural networks. These networks detect stance/swing transitions provide proper assistance at the desired timing during variable-speed walking [12,17]. For mid-level control, some end-to-end data-driven methods have emerged. They demonstrate superior robustness across diverse individuals and environments [18,19]. These models leverage continuous physiological states as input and biological joint moments as output to enable real-time torque adaptation. However, despite their superior in flexibility, such end-to-end data-driven approaches are notoriously "data-hungry," requiring vast quantities of high-quality training data for deep learning architectures.

To collect biomechanical ground-truth labels, users must perform diverse tasks in laboratories equipped with motion capture (kinemetics) and force plates (ground reaction forces). And then, musculoskeletal-based OpenSim inverse dynamics were used to calculate joint moments [20–22]. Given the labor-intensive and complex nature of this process, researchers often rely on limited online datasets [19,23,24]. Concurrently, simulation-based synthetic data generated by advanced generative models presents a promising alternative. This paradigm has been firmly established in robotic locomotion and manipulation, which require accurate latent dynamics [25,26]. Recent studies leveraged data-driven reinforcement learning (RL) from scratch in simulation [27]. These versatile control policy overcomes the formidable sim2real gap using dynamics-aware models [28–31]. Although RL effectively learns motor skills via reward signals, current applications typically deploy the policy merely as a controller. Consequently, they neglect the policy's potential as a research platform. Specifically, the implicit dynamics encoded within the policy could serve as a powerful tool for data generation and validation [32].

Inspired by this concept , we trained a stylized walking agent in simulation to generate massive synthetic datasets with precise annotations parallelly. We obtained graceful and life-like walking behaviors for physically simulated characters via Adversarial Motion Priors (AMP) [33–35]. The generated synthetic data includes both sensor readings and torque profiles. A rigorous validation of the walking agent against experiment with OpenSim standard pipeline was made. The generated torque curves closely match the reference standards at a high degree of consistency, indicating the agent successfully learns walking dynamics from the reference motions. Then, we proposed a novel CNN-Transformer framework. Convolutional Neural Networks (CNNs) extract robust local features, while transformers capture long-range temporal dependencies. Together, they enable precise mapping of variable-length torque profiles. This approach was implemented on an autonomous ankle exoskeleton. The system ensured adaptability across walking speeds from 0.6 $m \cdot s^{-1}$to 1.75 $m \cdot s^{-1}$ at torque accuracy about 85%. We demonstrate that this task-agnostic controller accurately estimates user joint moments online and significantly reduces metabolic cost and lower-limb biological joint work during variable-speed walking, marking a critical step of exoskeleton technologies.

2. Materials and Methods

2.1. The Simulation Environment and Exoskeleton Hardware Architecture

All simulations were executed on a workstation equipped with an Nvidia RTX 6000 Ada Generation GPU (Driver version: 580.126.09, CUDA v12.9.41). The simulation framework utilized Isaac Sim (v4.5.0) integrated with PyTorch (v2.5.1+cu118) for deep learning training and validation. Biomechanical modeling and analysis were conducted using OpenSim (v4.5). To acquire ground-truth kinematic and kinetic data, we employed an optical motion capture (NOKOV, Mars 1.3H) synchronized with high-fidelity force plates (Bertec, FP4060).

The custom-developed ankle exoskeleton platform comprises a 1-dof system for each leg driven by a Xiaomi CyberGear motor. The embedded controller (d-robotics, RDK X5) operated at a frequency of 500 Hz to ensure real-time responsiveness. Proprioceptive sensing is achieved through

 doi:10.20944/preprints202603.2037.v1

a multi-sensor configuration: IMU (Yesense, YIS320, 200Hz), encoder (ZeroErr, eCoder 11, 1000Hz), 940 nm Laser ToF (NooPLoop,TOFSense-F/F2, 50 Hz).

2.2. Human-Stylized Gait and Torque Prediction Algorithm

We implemented the AMP algorithm within the Isaac Lab framework. The human model was configured with anthropometric parameters corresponding to a male subject (height: 180 cm, mass: 70 kg). Segment lengths and circumferences were derived from direct physical measurements, modeled in SolidWorks, and exported to URDF format using the SW2URDF plugin before conversion to USD for simulation deployment. Reference motion trajectories for the AMP policy were captured using an optical motion capture. This reference trajectories were also used for OpenSim inverse dynamics solving. After data preprocessing and cleaning, these trajectories were retargeted to the simulated model. To enable command-following capabilities, an additional reward term penalizing deviation from target velocity commands was incorporated into the training objective. All simulation data were acquired directly via the native Isaac Lab interfaces.

The proposed algorithm, termed CNN-Transformer, employs a hybrid encoder-decoder architecture integrating feature extraction with attention-based sequence modeling. Input sensor data (8 channels) are first processed by a CNN encoder which downsample the input and expand the feature dimension to 128. The extracted features are then fed into a Transformer Encoder consisting of three identical layers. Each encoder layer utilizes multi-head self-attention and a position-wise feed-forward network (hidden dimension 512), stabilized by layer normalization and dropout ($p = 0.1$). Subsequently, a Transformer Decoder, also composed of three layers, refines these representations through masked self-attention and cross-attention mechanisms. Finally, the decoded features are projected via a fully connected linear layer to generate a scalar torque prediction.

3. Results and Discussion

This work leverages advanced imitation learning and physics-based simulation environments to facilitate a paradigm shift from complex dynamic models toward data-driven biomechanical estimation. An algorithmic framework is established based on the principles of human bilateral coordinated locomotion, with subsequent deployment and experimental validation. First, detailed kinematic and kinetic parameters are generated based on human body characteristics, and model files are created for simulation training (Fig. 1a). The kinetic data for each link i comprise the inertial parameter vector $\mathbf{\Phi}_i=[m_i, m_ir_{xi}, m_ir_{yi}, m_ir_{zi}, I_{xxi}, I_{xyi}, I_{xzi}, I_{yyi}, I_{yzi}, I_{zzi}]^T$, and viscous friction coefficients $\mathbf{F}_{vi}$, Coulomb friction coefficients $\mathbf{F}_{ci}$, motor inertia parameters $\mathbf{B}_i$ etc. The kinematic data includes the kinematic coordinate and lower-limb gait data acquired through optical motion capture, with the upper extremities simplified as a single rigid body. The collected gait data serve as reference motion priors for AMP-based learning. A massively parallel simulation environment concurrently runs 4,096 agents for training. The Adversarial Motion Prior (AMP) framework leverages a discriminator to distinguish between generated and reference motion distributions, thereby incentivizing the policy to produce behaviors that closely match the reference data distribution (Figure 1b). This adversarial training objective ultimately yields an AMP policy capable of human-like locomotion (Video S1). To mitigate overfitting, early stopping is employed based on validation performance.

 doi:10.20944/preprints202603.2037.v1

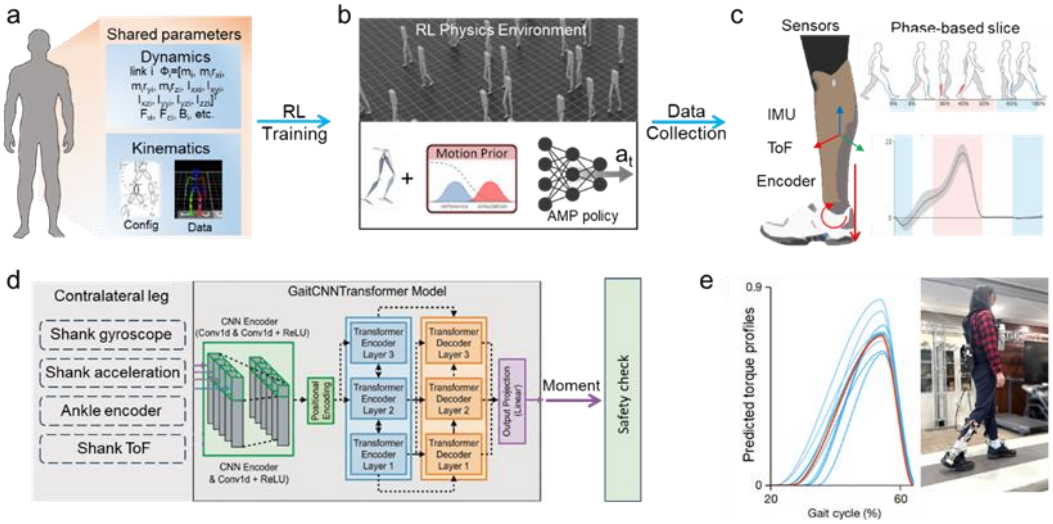

Figure 1. (a) Detailed kinematic and kinetic parameters based on human body for simulation training. **(b)** High-fidelity Isaac sim as a parallel RL training environment with AMP agent to imitate human-like gait with variable walking speeds. **(c)** Sensor inputs comprise IMU, Laser ToF, and encoder data, with specific mounting positions. The walking cycle was segmented, and ankle joint biomechanical torque profiles are obtained through OpenSim. **(d)** The CNN-Transformer algorithm with an encoder-decoder architecture, taking 8-dimensional data as input and safety check before motor execution**(e)**.

The sensor configuration was illustrated in Figure 1c. Sensor inputs comprise inertial measurement unit (IMU), laser time-of-flight (ToF), and encoder data. The design prioritizes sensor placement around the ankle joint to capture clinically relevant gait dynamics. Identical sensor types and mounting positions were adopted across simulation and experimental platforms, ensuring data fidelity and facilitating sim-to-real transfer. Gait cycle onset was defined by heel strike. In simulation, gait phase detection was implemented using supplemental plantar force sensors at the heel and metatarsal heads. For experimental deployment, an alternative phase recognition method intrinsic to the exoskeleton system was employed, which has been cross validated against optical motion capture data. As shown in Figure 1c, the proposed torque profile generation algorithm adopted an encoder-decoder architecture, taking 8-dimensional data as input. Convolutional neural networks (CNNs) performed feature extraction on the input data, while Transformer modules were employed for sequential torque prediction. The self-attention mechanism inherent to Transformers enabled the generation of variable-length output sequences, a characteristic that proved advantageous for real-time deployment across varying gait cycle durations. A non-real-time generation strategy was adopted for two primary considerations. First, computational overhead on embedded hardware was minimized. Second, pre-deployment safety check was enabled, allowing validation of generated torque profiles against predefined biomechanical constraints prior to actuation. The safety layer imposes hard constraints on cycle period adherence, peak torque clipping, and monotonicity check. Such precautionary measures were deemed essential for exoskeleton applications. Finally, the proposed torque prediction algorithm was deployed on a custom lower-limb exoskeleton platform for experimental validation. The system demonstrates robust generalization across variable walking velocities, with generated torque profiles exhibiting satisfactory tracking performance and biomechanical fidelity.

 doi:10.20944/preprints202603.2037.v1

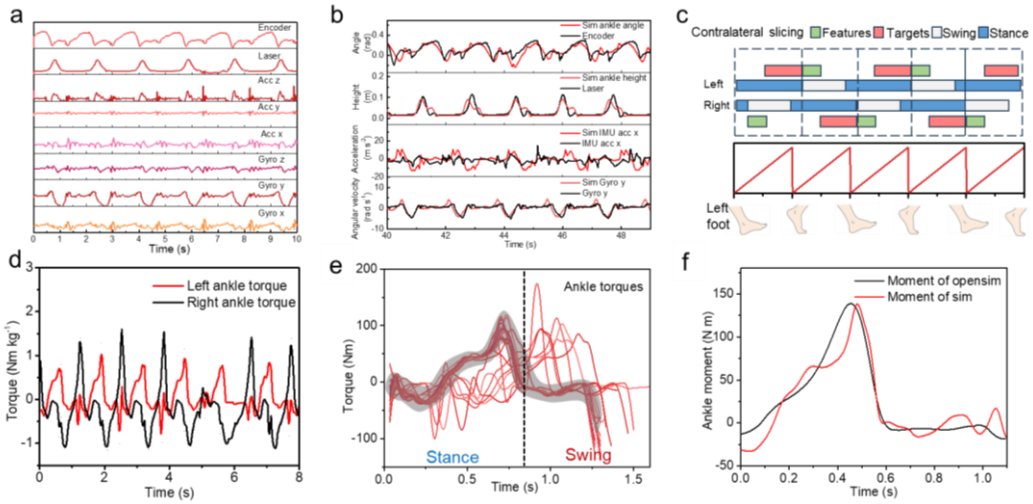

Figure 2. (a) Experimental sensor data at a walking velocity of 0.6 m·s^{-1}. **(b)** Sensor data comparison between the simulation and experiment at the same velocity. **(c)** Dataset construction workflow. Contralateral data are segmented in the footfall pattern, where contralateral swing phase (green) is utilized to generate stance phase torque profiles (red), . **(d)** Joint torque profiles of the left and right acquired in simulated walking. After segmentation, the high-fidelity of the simulation are evident in the stochastic variations of torque trajectories **(e)**. **(f)** Comparative analysis between simulation and experimental torque profiles (OpenSim pipeline).

Experimental data were acquired using the custom ankle exoskeleton platform, encompassing 8 sensor channels: joint angle encoders, laser time-of-flight (ToF) sensors for heel clearance estimation, and inertial measurement units (IMUs) capturing tri-axial acceleration and angular velocity as shown in Figure 2a. The gyro y corresponds to the sagittal plane of human body, the laser ToF distance corresponds to foot heel clearance to the ground, and the encoder corresponded synchronously. With the trained AMP agent of human-like gait in simulation environment, we cross-validated the above 4 channels data with experimental measurements. As shown in Figure 2b, the simulation not only preserves the characteristic, but also captures physically consistent details, such as the subtle peaks in the laser sensor signal etc. Figure 2c showed our dataset construction workflow, kinematic data of contralateral swing phase (green) was employed as the features input for CNN-Transformer. The upcoming stance-phase push-off torque of ankle joint (red) was collected as the target curve as shown in foot fall pattern in Figure 2c. The heel-strike event was utilized as the temporal onset for each gait cycle. Figure 2d showed the obtained ankle torque profiles, normalized to 70 kg body mass. The prominent positive peaks in the torque curves correspond to the active push-off phase, providing the necessary propulsive force to walk forward. We noted that discernible bilateral asymmetry and inter-cycle variability exists, inheriting stochasticity of the Isaac Sim physics engine. Rather than exhibiting rigid periodicity, the gait remains quasi-periodic, with no two cycles being identical. This characteristic ensured that the synthesized gait more closely approximates real-world human locomotion, where physiological fluctuations and environmental perturbations prevented exact cycle-to-cycle replication.

We collected about 50,000 trials, each encompassing a complete gaits including standing initiation, ten steps of steady-state walking, and final termination. Figure 2e presented the selected samples of a dataset. Joint torques exhibited consistency during steady-state walking, whereas minor deviations were observed in a subset of data corresponding to acceleration and deceleration phases. By deploying 4,096 agents in parallel, we amassed a substantial data within a few minutes. Besides enhanced realism and scalability, our simulation-based data generation strategy was rigorously validated against the conventional gold standard pipline. Typically, optical motion capture for kinematics and force plates for ground reaction forces (GRFs) were used to collect data. OpenSim with inverse dynamic pipeline was used to calculate joint torques. We compared a representative joint torque profile from the AMP agent during against OpenSim output as shown in Figure 2f. Given that both methods adopted the same motion capture data as input, the comparison is directly valid.

 doi:10.20944/preprints202603.2037.v1

The AMP-derived profiles exhibited richer high-frequency details across both stance and swing phases. We attribute the smoother OpenSim curves to the aggressive filtering required for inverse dynamics convergence, an artifact circumvented by our proposed approach.

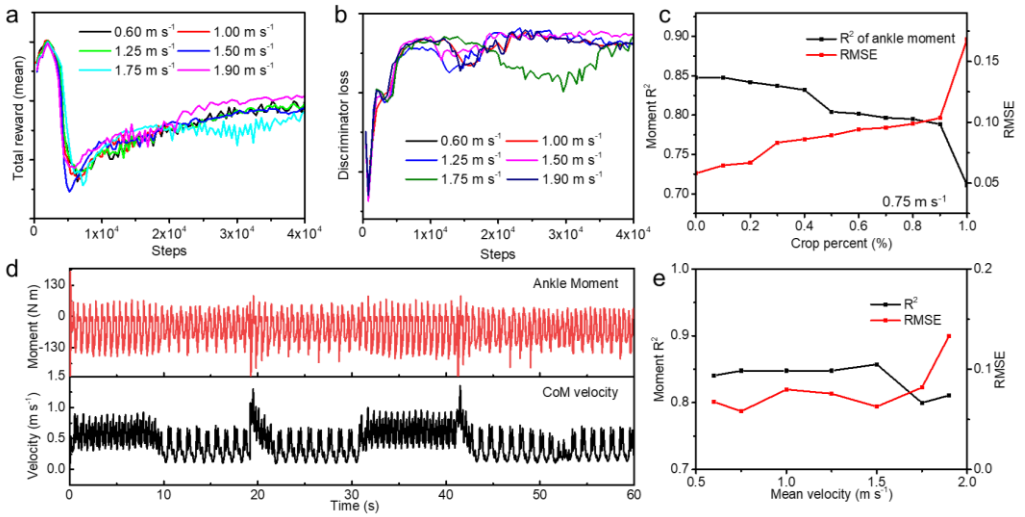

Figure 3. (a) At a broad velocities (0.6–1.9 m·s^{-1}), AMP agents exhibited consistent policy performance with converged training rewards. **(b)** The discriminator losses of the AMP agent across walking speeds. **(c)** Relationship between swing phase data cropping and prediction accuracy at 0.75 m·s^{-1}. **(d)** The CoM velocity and joint torques throughout in a walk episode, together with the accuracy characteristics of predicted torque profiles at varied walking speeds **(e)**.

Walking velocities in real-world scenarios exhibited significant variability, both between different trials and between individual steps. Consequently, we conducted a comprehensive evaluation to quantify the impact of velocity variations. Varied walking speed ranging from slow 0.6 m·s^{-1} to very fast 1.9 m·s^{-1} was studied. Extra reward terms were added into the total reward in AMP agent to endow velocity tracking ability. As shown in Figure 3a, the reward curves exhibited convergence, indicating that the policies effectively learned walking skills against speed variations. To prevent the erosion of human-like gait characteristics during high-velocity training, we increased the weights of the style reward, which penalized deviations from the reference dataset's behavioral style. This strategy ensured that the discriminator loss converged to comparable levels across all tested velocities (Figure 3b), confirming that the agent successfully preserved human motion characters. Reasonably, high walking velocities with shorter swing phases posed a challenge for temporal feature extraction. We conducted an ablation study at 0.75 m·s^{-1} by systematically truncating input data as shown in Figure 3c. The model maintained high accuracy with up to the last 40% swing phase data filled with 0. Conversely, when the input data was entirely absent (100% truncation), the algorithm defaulted to outputting expectation of all reference curves. Figure 3d show a representative walking trial, including the gait initiation, steady-state walking, and variable velocities, characterized by intermittent acceleration and deceleration. By directly extracting joint torque data, we observed that torques were minimal during slow walking but increased significantly during acceleration phases. Concurrently, the sagittal plane velocity of CoM was synchronously recorded to correlate with these dynamic torque variations as is shown in Figure 3d. We segmented joint torque profiles specifically within the push-off phase across complete gait cycles to evaluate prediction accuracy. The algorithm demonstrated robust performance across the velocities, maintaining high fidelity from slow to moderate speeds. However, a notable degradation in accuracy was observed at high velocities (1.75 m·s^{-1}). This decline was likely attributable to insufficient effective data points caused by the interaction between rapid gait dynamics and the sensor system's fixed sampling frequency (50 Hz), thereby limiting temporal resolution during fast locomotion.

 doi:10.20944/preprints202603.2037.v1

Subsequently, we deployed and validated the proposed CNN-Transformer prediction algorithm on our exoskeleton platform. The validation protocol involved variable-speed level walking on a footpath with force plate and optical motion capture, as shown in Figure 4a. The exoskeleton and sensor configuration were detailed in Fig. 4b; notably, the system employs a single motor to provide assistive torque at the ankle joint. Each experimental trial encompassed a comprehensive locomotion sequence: gait initiation, steady-state walking, intermittent acceleration, deceleration, and final termination. As illustrated in the representative data segment (Figure 4c), the joint torque profiles exhibited distinct variations corresponding to these dynamic gait transitions. The exoskeleton, governed by a phase-detection algorithm, delivered only plantarflexion torque during the push-off phase, as depicted by the red solid line in Figure 4c. Specifically, upon detection of the torque activation, the system executed proportional assistance based on the predicted torque profile. Given the motor's torque limits, the assistance gain was calibrated to 10% of the predicted profiles.

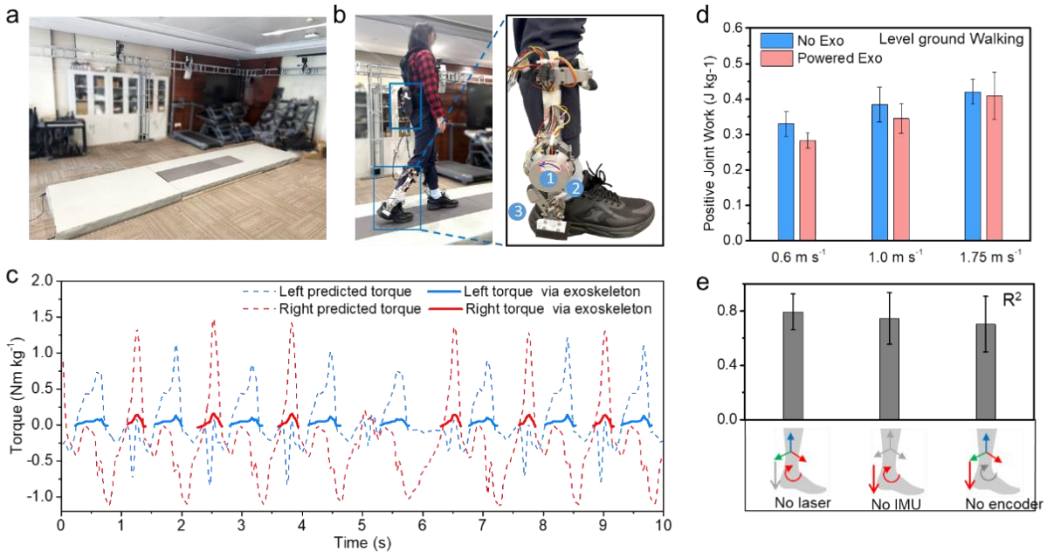

Figure 4. (a) Experimental setup comprised an optical motion capture and an instrumented walkway with force plates. **(b)** The exoskeleton device utilized for CNN-Transformer algorithm deployment, with integrated sensor placements aligned in simulation: (1) IMU, (2) ToF, and (3) encoder. **(c)** Predicted bilateral ankle joint torque profiles and the corresponding assistive torque delivered by the exoskeleton during variable-speed walking. **(d)** Reduction in human mechanical work attributable to exoskeleton assistance. **(e)** Variation in accuracy under conditions of partial sensor failure within our multi-sensor system.

To analyze the effect of our controller at the joint level, mechanical work was measured under the with exoskeleton and the without exoskeleton conditions. As shown in Figure 3d, the total positive mechanical work of the user's ankle joints (the sagittal plane) was significantly lowered with powered exoskeleton compared with no-exoskeleton condition during level ground walking [change of 0.046 J kg^{-1} at 0.6 $m{\cdot}s^{-1}$, 0.039 $J{\cdot}kg^{-1}$ at 1.0 $m{\cdot}s^{-1}$, and 0.011 $J{\cdot}kg^{-1}$ at 1.75 $m{\cdot}s^{-1}$]. Given the employment of multiple sensors in our setup, we investigated the performance of these sensors under a specific fault-tolerant condition, a critical consideration for safety in multi-sensor systems. By individually disabled each module, and applying corresponding dropout during training, we observed no significant degradation in accuracy. Notably, the encoder was found to play a vital role in torque estimation; its absence led to the substantial decline in accuracy (17%), suggesting that the encoder provided higher data quality and was more correlated with torque computation. Furthermore, during the human push-off phase, all three sensors generated responsive signals: the encoder directly captured joint angles, the IMU tracked the shank's pose, and the laser monitored foot-ground interaction. This demonstrates that our sensor system configuration possesses sufficient redundancy, thereby ensuring safety.

 doi:10.20944/preprints202603.2037.v1

4. Conclusions

This study establishes a unified, synthetic data-driven framework for ankle exoskeletons that effectively generalized across a broad walking velocity. Using massive parallel physics-based simulation, we generated high-fidelity biomechanical datasets from AMP agents, without labor-intensive artifacts filtering and conventional OpenSim inverse dynamics pipelines. We proposed CNN-Transformer architecture, which leveraged contralateral swing-phase sensor data to predict variable-length push-off torque profiles, demonstrating robust prediction accuracy and seamless sim-to-real transferability. Experimental validation confirmed that this controller significantly reduced user ankle positive mechanical work ranging from 0.6 $m \cdot s^{-1}$ to 1.75 $m \cdot s^{-1}$, thereby lowering metabolic demand. Furthermore, our multi-sensor configuration exhibited inherent fault tolerance; while encoder data proved most critical for precision, the complementary information from IMU and ToF sensors ensured safe, stable operation even under partial sensor failure. In the future, this synthetic data-driven paradigm will offer a scalable foundation for developing controllers capable of managing complex locomotor tasks and multi-joint coordinated assistance. Ultimately, this work demonstrated that scalable, data-driven approaches could replace rigid, handcrafted control strategies, offering a practical and adaptable pathway toward deploying data-driven exoskeletons in unconstrained, real-world environments.

Supplementary Materials: The following supporting information can be downloaded at: Preprints.org, Video S1: Diverse variable-speed walking scenarios in simulation used for data collection.

Author Contributions: Conceptualization, data curation, formal analysis, methodology, supervision, writing—draft preparation, J. S. & H. Z.; data curation, formal analysis, investigation, visualization, writing—draft preparation, writing—revision preparation, Y. Y. & B. L.; project administration, funding acquisition, X. W.; All authors have read and agreed to the published version of the manuscript.

Funding: This work was supported by the National Key R&D Program of China under the International Science and Technology Innovation Cooperation project "Home-based Wearable Multi-Channel Monitor and AI-assisted Diagnostic System Development and Applications (Grant No. 2023YFE0112600).

Institutional Review Board Statement: Not applicable.

Informed Consent Statement: Not applicable.

Data Availability Statement: All produced data are available within the manuscript.

Acknowledgments: The author would like to thank all the participants for their valuable input in this study.

Conflicts of Interest: The authors declare no competing interests.

References

1. Siviy, C. *et al.* Opportunities and challenges in the development of exoskeletons for locomotor assistance. *Nat. Biomed. Eng.* **2023**, 7, 456-472.
2. Slade, P. *et al.* On human-in-the-loop optimization of human–robot interaction. *Nature* **2024**, 633, 779-788.
3. Williams, J. R. *et al.* OpenExo: An open-source modular exoskeleton to augment human function. *Sci. Robot.* **2025**, 10, eadt1591.
4. Franks, P. W. *et al.* Comparing optimized exoskeleton assistance of the hip, knee, and ankle in single and multi-joint configurations. *Wearable Technologies* **2021**, 2, e16.
5. Prete, A. D. *et al.* Locomotion Mode Transitions: Tackling System-and User-Specific Variability in Lower-Limb Exoskeletons. *arXiv preprint arXiv:2411.12573* **2024**.
6. Kim, J. *et al.* Reducing the metabolic rate of walking and running with a versatile, portable exosuit. *Science* **2019**, 365, 668-672.
7. Zhang, J. *et al.* Human-in-the-loop optimization of exoskeleton assistance during walking. *Science* **2017**, 356, 1280-1284.

 doi:10.20944/preprints202603.2037.v1

8. Mooney, L. M., Rouse, E. J. & Herr, H. M. Autonomous exoskeleton reduces metabolic cost of walking. In 2014 36th Annual International Conference of the IEEE Engineering in Medicine and Biology Society, 26-30 Aug. 2014
9. Ding, Y., Kim, M., Kuindersma, S. & Walsh, C. J. Human-in-the-loop optimization of hip assistance with a soft exosuit during walking. *Sci. Robot.* **2018**, 3, eaar5438.
10. Koller, J. R., Jacobs, D. A., Ferris, D. P. & Remy, C. D. Learning to walk with an adaptive gain proportional myoelectric controller for a robotic ankle exoskeleton. *J. Neuroeng. Rehabil.* **2015**, 12, 97.
11. Slade, P., Kochenderfer, M. J., Delp, S. L. & Collins, S. H. Personalizing exoskeleton assistance while walking in the real world. *Nature* **2022**, 610, 277-282.
12. Kang, I. *et al.* Real-Time Gait Phase Estimation for Robotic Hip Exoskeleton Control During Multimodal Locomotion. *IEEE Robot. Autom. Let.* **2021**, 6, 3491-3497.
13. Medrano, R. L., Thomas, G. C., Keais, C. G., Rouse, E. J. & Gregg, R. D. Real-Time Gait Phase and Task Estimation for Controlling a Powered Ankle Exoskeleton on Extremely Uneven Terrain. *IEEE T. Robot.* **2023**, 39, 2170-2182.
14. Lee, D., Lee, S. & Young, A. J. AI-driven universal lower-limb exoskeleton system for community ambulation. *Sci. Adv.* **2024**, 10, eadq0288.
15. Laschowski, B., McNally, W., Wong, A. & McPhee, J. Environment Classification for Robotic Leg Prostheses and Exoskeletons Using Deep Convolutional Neural Networks. *Front. neurorobot.* **2022**, Volume 15 - 2021.
16. Qian, Y. *et al.* Predictive Locomotion Mode Recognition and Accurate Gait Phase Estimation for Hip Exoskeleton on Various Terrains. *IEEE Robot. Autom. Let.* **2022**, 7, 6439-6446.
17. Shepherd, M. K., Molinaro, D. D., Sawicki, G. S. & Young, A. J. Deep Learning Enables Exoboot Control to Augment Variable-Speed Walking. *IEEE Robot. Autom. Let.* **2022**, 7, 3571-3577.
18. Molinaro, D. D., Kang, I. & Young, A. J. Estimating human joint moments unifies exoskeleton control, reducing user effort. *Sci. Robot.* **2024**, 9, eadi8852.
19. Molinaro, D. D. *et al.* Task-agnostic exoskeleton control via biological joint moment estimation. *Nature* **2024**, 635, 337-344.
20. Delp, S. L. *et al.* OpenSim: Open-Source Software to Create and Analyze Dynamic Simulations of Movement. *IEEE Trans. Biomed. Eng.* **2007**, 54, 1940-1950.
21. Dembia, C. L., Bianco, N. A., Falisse, A., Hicks, J. L. & Delp, S. L. OpenSim Moco: Musculoskeletal optimal control. *PLoS Comput. Biol.* **2021**, 16, e1008493.
22. Seth, A. *et al.* OpenSim: Simulating musculoskeletal dynamics and neuromuscular control to study human and animal movement. *PLoS Comput. Biol.* **2018**, 14, e1006223.
23. Exoskeleton Gait Dataset, Available online: <https://simtk.org/projects/exo-gait>.
24. Embry, K. R., Villarreal, D. J., Macaluso, R. L. & Gregg, R. D. Modeling the Kinematics of Human Locomotion Over Continuously Varying Speeds and Inclines. *IEEE Trans. Neural Syst. Rehabil. Eng.* **2018**, 26, 2342-2350.
25. Zhang, K. *et al.* Generative artificial intelligence in robotic manipulation: A survey. *arXiv preprint arXiv:2503.03464* **2025**.
26. Gu, Z. *et al.* Humanoid Locomotion and Manipulation: Current Progress and Challenges in Control, Planning, and Learning. *arXiv:2501.02116* **2025**.
27. Luo, S. *et al.* Experiment-free exoskeleton assistance via learning in simulation. *Nature* **2024**, 630, 353-359.
28. Salvato, E., Fenu, G., Medvet, E. & Pellegrino, F. A. Crossing the Reality Gap: a Survey on Sim-to-Real Transferability of Robot Controllers in Reinforcement Learning. *IEEE Access* **2021**, 9, 153171-153187.
29. Wang, M. & Luo, S. Predicting Human Locomotion in Reduced Gravity via Deep Learning-Driven Musculoskeletal Simulation. *IEEE Robot. Autom. Let.* **2026**, 11, 3899-3906.
30. You, Z. & Zhou, X. Exoskeleton Control through Learning to Reduce Biological Joint Moments in Simulations. *arXiv preprint arXiv:2603.07629* **2026**.
31. Zhu, H., Xu, Y., Zhou, Z., Gao, Y. & Ding, N. Inertial Parameters Identification for Floating-Base Multibody Systems Using Spinning Trajectories. In 2025 IEEE 23rd International Conference on Industrial Informatics (INDIN), 12-15 July 2025

 doi:10.20944/preprints202603.2037.v1

32. Ijspeert, A. J., Crespi, A., Ryczko, D. & Cabelguen, J.-M. From Swimming to Walking with a Salamander Robot Driven by a Spinal Cord Model. *Science* **2007**, 315, 1416-1420.
33. Ma, L. *et al.* StyleLoco: Generative Adversarial Distillation for Natural Humanoid Robot Locomotion. *arXiv:2503.15082* **2025**.
34. Escontrela, A. *et al.* Adversarial Motion Priors Make Good Substitutes for Complex Reward Functions. In 2022 IEEE/RSJ International Conference on Intelligent Robots and Systems (IROS), 23-27 Oct. 2022
35. Peng, X. B., Ma, Z., Abbeel, P., Levine, S. & Kanazawa, A. AMP: adversarial motion priors for stylized physics-based character control. *ACM Trans. Graph.* **2021**, 40, 144.